International Symposium
On Turbulence and Shear Flow
Phenomena (TSFP-9)
June 30 - July 3, 2015 *Melbourne, Australia*

TRACKING COHERENT STRUCTURES IN MASSIVELY-SEPARATED AND TURBULENT FLOWS

Yangzi Huang, Matthew Rockwood, & Melissa A. Green
Department of Mechanical and Aerospace Engineering
Syracuse University
Syracuse, NY
greenma@syr.edu

ABSTRACT

Coherent structures are tracked in three simulations of massive-separated or turbulent flow. Topological saddle points are found using intersections of the postive- and negative-time Lagrangian coherent structures, and these points are then followed as the flow evolves in order to track individual structures. In the cases of a 2D flat plate undergoing a 45° pitch-up maneuver and a circular cylinder in cross-flow, tracking saddle points showed a rapid acceleration of the structure as it shed from the plate or cylinder surface. For a simulation of wall-bounded turbulence in a channel flow, tracking the LCS saddle points shows that average structure convection speed exhibits a similar trend as a function of wall-normal distance as the mean velocity profile.

INTRODUCTION

Coherent structures are a key component of unsteady flows such as propulsive wakes, flow separation, and instabilities in shear layers. They play a key role in fluid mixing and instabilities, kinetic energy production and dissipation, mass transport and diffusion, frictional drag, and others. The visualization and tracking research of vortices helps to explain the basic physics of turbulent motions, and to improve turbulent flow modeling, prediction, and control design and implementation. Consequently, it can aid in the design of high-lift devices, mixing progress in power engines, or artificial adaption of biological flexible control surfaces.

Although vortex research has been carried on for decades, a widely-accepted, objective definition of a vortex and its boundaries remains unrealized. Improvement of experimental techniques has led to larger amounts of data, requiring development of automated procedures for vortex tracking (Chong *et al.*, 1990). Many vortex criteria identify the structures by a a local swirling motion, which has the presence of closed or spiral streamlines or pathlines in a suitable reference frame. Graftieaux *et al.* (2001) initially defined a scalar function Γ_1 by using the topology of the velocity field to yield the center of the vortex core. The Q criterion, from Hunt *et al.* (1988), identifies regions as vortices if the norm of the local rate of rotation tensor is dominant over the norm of the local rate of strain.

Alternatively, Lagrangian coherent structures (LCS) analysis is a Lagrangian method based on the quantities calculated along fluid particle trajectories. LCS are identified as maximizing ridges of the scalar finite-time Lyapunov exponent (FTLE), and these ridges have been shown to represent structure boundaries in vortex dominated flows (Haller, 2001, 2002). This calculation can be done in both positive- and negative-time, yielding material lines boundaries that either locally separate or repel trajectores (positive-time, pLCS) or locally attract trajectories (negative-time, nLCS).

METHOD

Γ_1

In the current work, coherent structures are tracked using Γ_1, the Q criterion, and LCS. Graftieaux et al. initially defined the scalar function Γ_1 by using the topology of the velocity field to yield the center of the vortex core (Graftieaux *et al.*, 2001). The velocity field is sampled at discrete spatial locations, and the Γ_1 quantity is defined as,

$$\Gamma_1(P) = \frac{1}{N}\sum_{i=1}^{N}\frac{(\mathbf{PM}\times\mathbf{U}_M)\cdot\mathbf{z}}{||\mathbf{PM}||\cdot||\mathbf{U}_M||}dA = \frac{1}{N}\sum_{i=1}^{N}\sin(\theta_M)dA, \quad (1)$$

where A is a rectangular domain of fixed size and geometry, centered on P, and M lies in S.

Here, N is the number of points M inside A, and z is the unit vector normal to the measurement plane. θ_M is the angle between the velocity vector U_M and the radius vector PM, and $||\cdot||$ represents the Euclidean norm of the vector. The parameter N plays the role of a spatial filter, but only weakly affects the location of the maximum Γ_1. The location is determined by local maximum, typically ranging from 0.9 to 1 near the vortex center. The Γ_1 function provides a simple and robust way to identify the locations of centers of vortical structures. It is, however, not Galilean invariant, and therefore is dependent on the convection speed of any structures of interest.

Q-criterion

Another Eulerian scalar, the Q criterion, identifies regions as vortices if the norm of the local rate of rotation tensor is dominant over the norm of the local rate of strain (Hunt *et al.*, 1988). The velocity gradient tensor $\nabla\mathbf{u}$ is decomposed into the symmetric rate of strain tensor S and antisymmetric rate of rotation tensor Ω, as,

$$\nabla\mathbf{u} = S + \Omega, \quad (2)$$

where $S = \frac{1}{2}[\nabla \mathbf{u} + (\nabla \mathbf{u})^T]$ and $\Omega = \frac{1}{2}[\nabla \mathbf{u} - (\nabla \mathbf{u})^T]$.

The Q criterion is then defined as,

$$Q = \frac{1}{2}[||\Omega||^2 - ||S||^2] > 0. \quad (3)$$

Here, $||\Omega||$ represents the Euclidean norm of the local rate of rotation tensor and $||S||$ represents the Euclidean norm of the local rate of strain tensor S. A vortex is defined in those regions where $Q > 0$, which is interpreted as a dominance of rotation over strain.

A vortex core is found using the Q criterion in two ways. In the case of the flat plate, we first identify a rectangular area around the Γ_1 core point that roughly bounds the vortex. The center is then found as the "center of mass" of Q in that rectangular region. This allows us to simultaneously consider the multiple vortices that are present in the simulation. In the case of the circular cylinder, the point of maxiumum Q in the region close the cylinder surface is used.

Lagrangian coherent structures

Our method to identify Lagrangian coherent structures uses the maximizing ridges of the scalar finite-time Lyapunov exponent field (FTLE), as these ridges have been shown to represent structure boundaries in vortex dominated flows (Haller, 2001, 2002). The FTLE value measures the maximum rate of separation around a certain location in space ($\mathbf{x_0}$) by first calculating the flow map of neighboring particles $\phi(\mathbf{x_0}, t_0, T)$ over an integration time T, and constructing the Cauchy-Green strain tensor from the spatial gradient of the flow map. The maximum eigenvalue of the Cauchy-Green strain tensor is referred to as the coefficient of expansion σ_T.

$$\sigma_T(\mathbf{x}_0, t_0) = \lambda_{max}\left(\left[\frac{\partial \phi(\mathbf{x}_0, t_0, T)}{\partial \mathbf{x}_0}\right]^T \left[\frac{\partial \phi(\mathbf{x}_0, t_0, T)}{\partial \mathbf{x}_0}\right]\right). \quad (4)$$

From there, the FTLE field is defined from the coefficient of expansion as,

$$FTLE_T(\mathbf{x}_0, t_0) = \frac{1}{2T}\log\sigma_T(\mathbf{x}_0, t_0). \quad (5)$$

Maximizing ridges in this field indicate high levels of Lagrangian stretching among nearby particle trajectories.

This calculation can also be done by calculating particle trajectories initialized at t_0 in negative-time. This calculation will also yield a scalar FTLE field, and because it measures Lagrangian separation in negative time, its ridges represent those regions in the flow where particle trajectories are currently being attracted. By including ridges from both FTLE calculations, the analysis produces both the repelling material lines along which particle trajectories locally separate from each other (positive-time, pLCS) or attracting material lines along which particle trajectories locally contract to each other (negative-time, nLCS). The pLCS and nLCS intersect at the outer boundaries of vortices but don't overlap. Inclusion of both LCS provides a more complete boundary delineating which particles are entrained into the vortex from those that continue to convect with the outer flow.

To track vortex structures using the LCS, we use not the full ridges of the FTLE fields, but those points where the nLCS intersect with the pLCS. These intersections of the attracting and repelling material lines in the flow are effective saddle points, and have been shown to be dynamically important features of the vortex boundaries (Green *et al.*, 2011).

RESULTS

2D plate in pitch-up maneuver

Leading edge and trailing edge vortex center tracking is demonstrated on data from the simulation of a flat plate undergoing a 45° pitch-up maneuver (Eldredge, 2007). Figure 1 shows an example of where each method identifies its tracking target. This instant of time is well after the leading-edge vortex has developed, and multiple vortices have shed from the trailing edge. Both Γ_1 cores (yellow dots) and Q centers (green dots) locate the vortex centers in approximately the same location. The green boxes illustrate the region in which the center of Q was found, demonstrating that a reasonably large area of the vortex was considered. As described, the cyan dots locate the saddle points at the intersections of the pLCS (blue) and nLCS (red).

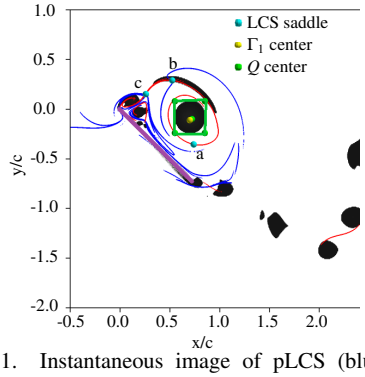

Figure 1. Instantaneous image of pLCS (blue), nLCS (red), with contour level of values more than 85% maximum, and positive Q criterion (black) with contour level at 0 in the wake of the panel pitching up, with identified tracking markers labeled. Flat plate is plotted as purple line. A green box is to mark the region where the center of Q was found

Figure 2 shows the location of each of these tracking targets in time ($t^* = tU_\infty/c$), measured as distance from the leading edge and scaled by the plate chord. From this figure, we see that Q and Γ_1 give very similar tracks of the vortex core. The tracks of the LCS saddles, on the other hand, appear to move with a different profile. As can be seen in movies of the tracking center evolutions, some of this is because of the rotation of the structures as they evolve downstream, meaning that boundary of the structure (including the saddle) will trace out a larger track than the vortex core. A portion of the difference, however, also comes from the fact that as the a structure grows, the core might shift downstream even as it remains attached to the plate. This piece of information is available in the track of saddle "a," which is part of the boundary of the primary leading-edge vortex that first forms and sheds. As shown in the cyan diamonds in figure 2, the saddle moves away from the leading edge

slowly, with a rapid acceleration around $t^* = 2.5$. The two relatively distinct phases of constant motion are highlighted with red lines in figure 2. We propose that this rapid acceleration of the saddle points from structures with longer formation times gives a good indication of the timing of vortex shedding.

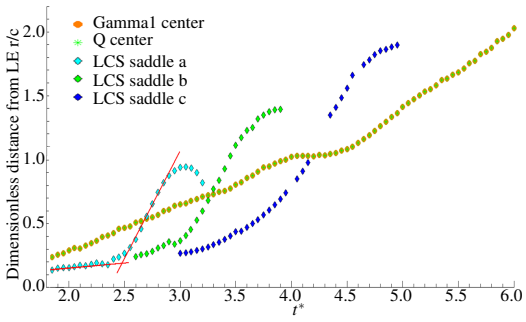

Figure 2. Distance of tracking markers, measured from the panel leading edge, in time. (Red lines indicate the relative slopes of saddle point a motions in time.)

Cylinder in cross-flow

A similar saddle track is observed in periodic vortex shedding from a circular cylinder as described by Rockwood & Green (2014). These FTLE fields were generated using velocity data from a two-dimensional immersed boundary simulation by Colonius & Taira (2008). The flow maps were calculated using integration times of two shedding periods (T).

As seen in the top of figure 3, the FTLE ridges in this flow are also intertwined in a system of interconnected saddles. The intersection highlighted by the black arrow in that figure is a saddle that resides on the cylinder surface while the adjacent vortex structure continues to form. Approximately 0.4 T later, the saddle has departed from the cylinder surface, as seen in the bottom image of figure 3.

Rockwood & Green (2014) tracked this saddle by hand and showed that as the vortex is initially forming, it remains stationary and attached to the cylinder surface. As the vortex sheds, it abruptly accelerates from the cylinder surface. This result is shown in figure 4. Here, the black lines give an indication of the near-zero motion of the saddle at early times in the vortex shedding period, while the structure is still attached and forming. Near $t/T = 0.8$, the saddle accelerates to a new constant velocity, which is the same as the velocity of the vortex core point (as identified by Q_{max}), and can be considered the vortex convection velocity. This decomposition of the saddle motion into two phases of relatively constant motion is similar to the pitch-up plate, as shown by the red lines in figure 2.

Turbulent structure tracking

Similar saddle point tracking is used in the case of a three-dimensional, fully turbulent channel simulation, generated using the method of Kim *et al.* (1987). FTLE fields in this data were originally presented in Green *et al.* (2007). Previous work identifies the saddles by hand, while current work manages to detect and track them automatically from processed FTLE data sets. Figure 5 shows flow in a 2D

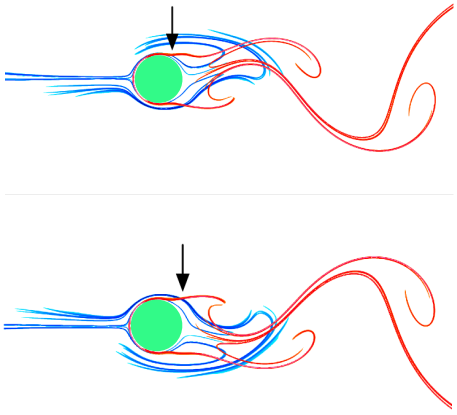

Figure 3. Instantaneous snapshot of positive- and negative-time LCS (blue and red, respectively) in the flow around a circular cylinder (represented by a green circle). Saddle point recently shed from the top half of the cylinder is highlighted by a black arrow.

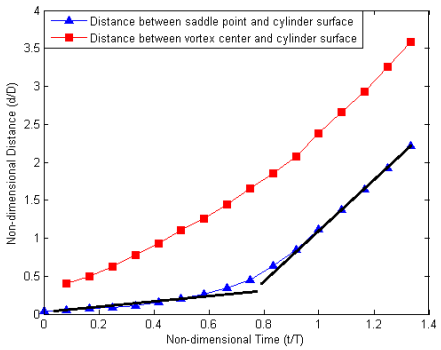

Figure 4. Distance of vortex from cylinder surface. Red squares: distance from surface to vortex core, taken as point of maximum Q criterion inside the vortex. Blue triangles: distance from cylinder surface to LCS saddle. Black lines indicate the relative slopes of the saddle motions in time.

plane cutting from turbulent channel at $t^* = 6000$, where time is nondimensionalized as, $t^+ = Tu_\tau^2/\nu$, with u_τ as the friction velocity, and ν as the kinematic velocity. Distance from the wall is represented as $y^+ = u_\tau y/\nu$, and the location of the plane of calculation in figure 5 is $y^+ = 49$. The flow map integration time is $T^+ = 27$. Negative- and positive-time LCS, are shown as red and blue curves, respectively, and cyan dots locate the saddle points at the intersections of the pLCS and nLCS.

The ridges of the FTLE field are codimension 1 structures, meaning that in two-dimensional flows, they are one-dimensional curves. In the case of the turbulent channel, which is three dimensional, the FTLE ridges will be two-dimensional curved surfaces in space. In figure 5, although the flow maps were only calculated in a single plane, they were advected in the full three-dimensional data domain. For this reason, the ridges in figure 5 can be considered the intersection of the 2D surfaces of the LCS with this particular plane at $y^+ = 49$. The saddles, which are the intersec-

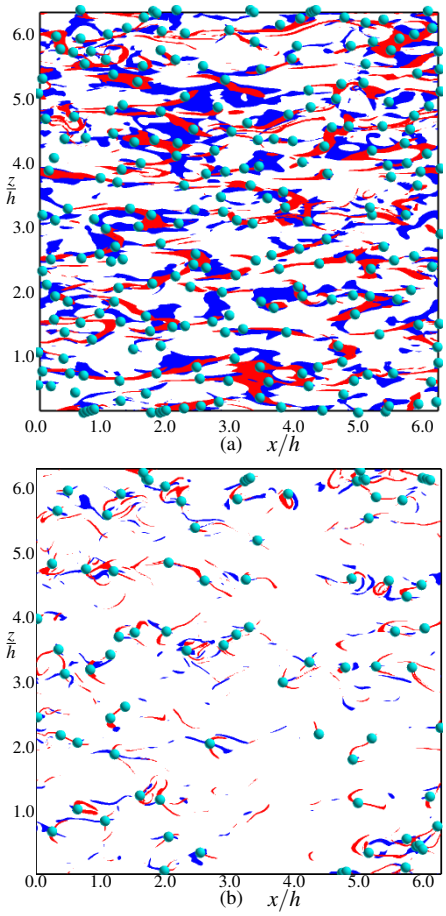

Figure 5. Instantaneous snapshots of positive- and negative-time LCS (blue and red, respectively) in the turbulent channel simulation. Saddle points are highlighted by cyan circles.

tions of the LCS, are then naturally codimension 2, meaning that they are zero-dimensional points in 2D flows, and one-dimensional line segments in 3D flows. The saddle points of figure 5 are then intersections of the saddle curves with the 2D plane.

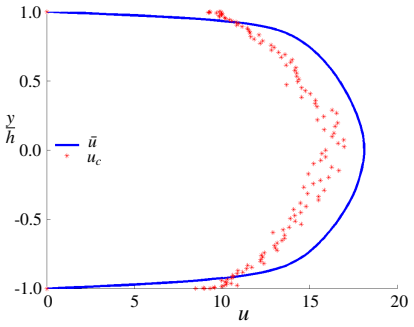

Figure 6. Plane-averaged velocity of saddles points in the turbulent channel simulation, plotted against wall-normal distance (red). This data is compared with the simulation mean streamwise velocity profile (blue).

FTLE ridges and saddles were identified for a series of ten time-resolved snapshots, at 129 planes across the channel width. Using a cross-correlation algorithm, an average streamwise velocity of saddles at each plane was then calculated, with dimensionless average tracking velocity $u_c = u/u_\tau$. In figure 6, this averaged structure convection velocity, found by tracking the LCS saddles, is shown as a function of wall-normal distance. For comparison, the channel mean streamwise velocity $\bar{u}$ is also included on the same axes. The structure convection velocity u_c is less than the mean profile velocity $\bar{u}$ for -0.914 $< y/h <$ 0.924 ($y^+ < 15.5$ and $y^+ < 13.7$, respectively). This is shown directly in figure 7, which shows the velocity deficit, calculated as, $\Delta u = (\bar{u} - u_c)/\bar{u}$. In the region where $\bar{u} > u_c$, the velocity deficit is on the order of 10% - 15%.

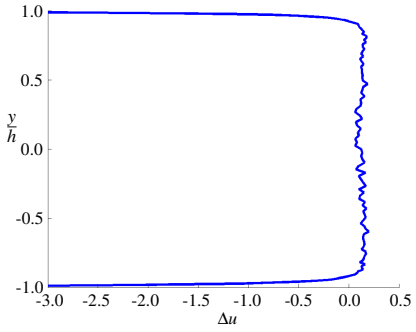

Figure 7. Velocity deficit of saddles tracking velocity and mean streamwise velocity in the turbulent channel simulation, plotted against wall-normal distance.

Close to the wall, $y^+ < 15.5$ or $y^+ < 13.7$, the velocity of the coherent structures as identified by the LCS saddles is larger than the channel mean profile velocity. While this is consistent with the physical interpretation that coherent structures will travel faster than the viscous-dominated mean velocity close to the wall, the data in that region may not be statistically converged. This is due to the thicker FTLE ridges in the planes closer to the wall, which may be a result on the flow map integration time. The longer times used to capture the larger scale structures across the channel may be suitable for the smaller scale structures near the wall. This will be addressed in future work.

SUMMARY

In all three applications, using the LCS saddles to track the structures yields an objective point in space to target, which enables us to start to develop automatic tracking algorithms after the computation of the requisite FTLE fields. In massively-separated flows such as leading edge vortex separation on a flat plate pitching up or vortex shedding off a circular cylinder, tracking the saddles allows for identification of an acceleration that can indicate shedding of the relevant vortex. In a turbulent channel simulation, tracking the objective saddle points provides the possibility of automatic tracking algorithm that will provide statistical quantities of coherent structure dynamics.

ACKNOWLEDGMENTS

This work was supported by the Air Force Office of Scientific Research under AFOSR Award No. FA9550-14-

1-0210.

REFERENCES

Chong, MS, Perry, A Eo & Cantwell, BJ 1990 A general classification of three-dimensional flow fields. *Physics of Fluids A: Fluid Dynamics (1989-1993)* **2** (5), 765–777.

Colonius, Tim & Taira, Kunihiko 2008 A fast immersed boundary method using a nullspace approach and multi-domain far-field boundary conditions. *Computer Methods in Applied Mechanics and Engineering* **197** (25–28), 2131 – 2146.

Eldredge, Jeff D 2007 Numerical simulation of the fluid dynamics of 2d rigid body motion with the vortex particle method. *J. Comput. Phys.* **221**, 626–648.

Graftieaux, Laurent, Michard, Marc & Grosjean, Nathalie 2001 Combining piv, pod and vortex identification algorithms for the study of unsteady turbulent swirling flows. *Measurement Science and Technology* **12** (9), 1422.

Green, Melissa A., Rowley, Clarence W. & Haller, George 2007 Detection of Lagrangian coherent structures in three-dimensional turbulence. *Journal of Fluid Mechanics* **572**, 111–120.

Green, Melissa A., Rowley, Clarence W. & Smits, Alexander J. 2011 The unsteady three-dimensional wake produced by a trapezoidal pitching panel. *Journal of Fluid Mechanics* **685**, 117–145.

Haller, George 2001 Distinguished material surfaces and coherent structures in 3d fluid flows. *Physica D* **149**, 248–277.

Haller, George 2002 Lagrangian coherent structures from approximate velocity data. *Physics of Fluids* **14** (6), 1851–1861.

Hunt, Julian CR, Wray, AA & Moin, Parviz 1988 Eddies, streams, and convergence zones in turbulent flows. In *Studying Turbulence Using Numerical Simulation Databases, 2*, , vol. 1, pp. 193–208.

Kim, John, Moin, Parviz & Moser, Robert 1987 Turbulence statistics in fully developed channel flow at low reynolds number. *J. Fluid Mech.* **177**, 133–166.

Rockwood, Matthew P. & Green, Melissa A. 2014 Lagrangian coherent structure analysis of vortex shedding in the wake of a cylinder. *Journal of Fluid Mechanics* (submitted).